

Cosmos caudatus extract-intervened zinc oxide nanoparticles: reaction mechanism, molecular docking, and optical properties

Indah Riwayati¹, Suci Madhania¹, Sugeng Winardi¹, Manabu Shimada², Kusdianto^{1*}

¹ Chemical Engineering Department, Institut Teknologi Sepuluh Nopember, Kampus ITS Sukolilo, Surabaya 60111, Indonesia

² Chemical Engineering Program, Graduate School of Advanced Science and Engineering, Hiroshima University, 4-1, Kagamiyama 1-chome, Higashi-Hiroshima, Hiroshima 739-8527, Japan

ABSTRACT

Zinc oxide nanoparticles (ZnO NPs) are extensively applied in numerous domains, including photocatalytic, antibacterial, anti-inflammatory, and anticancer applications. Utilization of ZnO NPs in numerous domains has generated increasing demand. Therefore, it is imperative to consider an economical, highly efficient, and sustainable approach. One plausible method for accomplishing these criteria is biological. This study aimed to investigate the reaction mechanism and physical, chemical, morphological, and optical characteristics of ZnO NPs emanated from *Cosmos caudatus* leaf extract employing a bioreduction approach. Furthermore, molecular docking analysis was conducted to obtain insights into the specific interactions between ZnO NPs and proteins found within microbial cells. X-ray diffraction (XRD) validated the existence of ZnO NPs, bearing a mean crystallite diameter of 50.54 nm. The morphology observed through scanning electron microscopy (SEM) examination exhibited hexagonal-shaped particles with a relatively consistent size distribution. The maximum absorbance was noticed at 385 nm, characterized by a band gap of 3.04 eV. Molecular docking showed that the ligand (ZnO) bound to *Escherichia coli* and *Aspergillus niger* which possess bond energies of -3.4 kcal/mol and -2.6 kcal/mol, respectively, and *Staphylococcus aureus* with -2.3 kcal/mol.

Keywords: Band gap, Biological, *Cosmos caudatus*, Green synthesis ZnO nanoparticle

OPEN ACCESS

Received: June 4, 2024
Revised: July 15, 2024
Accepted: September 30, 2024

Corresponding Author:
Kusdianto
kusdianto@its.ac.id

 **Copyright:** The Author(s). This is an open access article distributed under the terms of the [Creative Commons Attribution License \(CC BY 4.0\)](https://creativecommons.org/licenses/by/4.0/), which permits unrestricted distribution provided the original author and source are cited.

Publisher:
[Chaoyang University of Technology](https://www.its.ac.id/)
ISSN: 1727-2394 (Print)
ISSN: 1727-7841 (Online)

1. INTRODUCTION

Nano-semiconductors exhibit better properties than macroscopic semiconductors. Nano-semiconductors have distinct characteristics that result from the influence of quantum mechanics on electron behaviour rather than classical physics. Reducing a semiconductor's size to a few nanometres confines electron movement in all three spatial dimensions. This confinement leads to a significantly high surface-to-volume ratio in nano semiconductors, which in turn greatly impacts their physical and chemical properties. Notably, this confinement increases reactivity and enhances surface effects. Furthermore, certain nano-semiconductors can experience a notable improvement in carrier mobility, which refers to the speed at which electrons and holes move through the material due to reduced scattering events. Through the engineering of nano-semiconductors, researchers can create materials with specific electronic properties tailored for specific applications. Additionally, nano-semiconductors can exhibit entirely

novel phenomena that are absent in bulk materials. An example of such nanoparticles is zinc oxide nanoparticles (ZnO NPs), which exhibit a diverse spectrum of optical and electrical properties and possess significant potential for application across many domains. Additional notable features of the material include a remarkable binding energy of 60 meV, a notable range of electron mobility spanning from 200 to 1000 cm²(Vs)⁻¹, favourable transparency, pronounced luminescence under ambient settings when compared to TiO₂, and a substantive band gap of 3.3 eV at 300 K (Kalam et al., 2022). The optoelectronic characteristics of ZnO nanostructures are remarkably affected by multiple factors, including shape, crystallinity, size, crystal defects, and impurity content (Agarwal et al., 2019).

ZnO NPs' features are popular in biomedical applications, especially antibacterial therapy. ZnO NPs eradicate a multitude of bacteria, viruses, and fungi. Applications of ZnO NPs are feasible for medical devices, dressings, and surfaces. ZnO NPs have the potential to induce apoptosis in cancer cells without causing any damage to uninfected cells. Nanoparticle surface modification increases selective toxicity, improving anticancer drugs. ZnO NPs are used to deliver cancer and diabetes medicines. Pharmaceutical applications benefit from encapsulating and releasing therapeutic compounds (Jiang et al., 2018). ZnO NPs are effective photocatalysts, especially when exposed to ultraviolet (UV) radiation to degrade organic contaminants in water, and can be used to develop sensors for pollutant, gas, and other hazardous compound detection. ZnO NPs are advantageous in dye-sensitized solar cells (DSSCs) and perovskite solar cells due to their exceptional electron mobility and broad bandgap. In the energy generation field, ZnO NPs increase energy storage capacity in lithium-ion batteries. Sunscreens and other skin care products contain ZnO NPs to protect against UVA and UVB radiation, minimize skin irritation, and reduce inflammation. Semiconducting ZnO NPs are used in thin-film transistors, gas sensors, and other electronics. In food packaging, ZnO NPs reduce bacterial and fungal growth and retain freshness for food preservation (Debanath and Karmakar, 2013). For instance, Tangkawanit et al. (2023) employed ZnO NPs to enhance the textiles' thermal stability, colour fastness, and UV protection qualities. The antibacterial capabilities of ZnO allow for the inclusion of nanoparticles as an active element in polystyrene packaging (Thirugnanasambandan et al., 2023). ZnO NPs alloyed with Al₂O₃ can serve as a catalyst to degrade dibenzothiophene through oxidative desulfuration processes (Aabid et al., 2023). The use of ZnO NPs exhibits considerable potential across various domains, prompting the adoption of ecologically sustainable and cost-effective synthesis methods (Hudandini et al., 2022).

Chemical and physical processes, such as microwave radiation, sol-gel, hydrothermal, solvothermal, coprecipitation, and green synthetics, can be incorporated into ZnO NPs production (Kusdianto et al., 2021). Chemical synthesis typically produces hazardous compounds that are

neither readily degraded nor toxic as reduction or capping agents for producing ZnO NPs (Owais Mushtaq et al., 2022). Green synthesis is a technique for synthesizing ZnO NPs using phytochemicals, such as flavonoids, phenolics, terpenoids, saponins, and vitamins found in plant extracts, as complexing agents, capping substances, and stabilizers. Several research studies have demonstrated the successful use of diverse botanical extracts to produce ZnO NPs. Notable examples include *Acalypha fruticosa* L (Vijayakumar et al., 2020), *Alchemilla vulgaris* (Rajendrachari et al., 2021), *Euphorbia hirta* (Ahmad and Kalra, 2020), *Syzygium cumini* (Sadiq et al., 2021), *Nilgiriantsuciliantus* (Resmi et al., 2021), *Abutilon Indicum* and *Tectona grandis* (Eswari et al., 2022), and *Muntingia calabura* (Vinayagam et al., 2022).

Typically, the synthesis of ZnO NPs through bio-reduction utilizing plant extracts entails the process of obtaining a plant extract. The plants are washed with water and dried, and the desired compounds are subsequently extracted using solvents. The precursor acts as a source of zinc ions and plant chemicals for the formation of precipitates, which will be subjected to calcination to generate ZnO NPs. The ZnO produced is influenced by the phytochemical substances found in each species of plant. The generation of ZnO NPs using plant extracts is influenced by the content of the extract, precursors, pH, and calcination temperature. Various factors will have a substantial impact on the characteristics of ZnO NPs (Zeghoud et al., 2022).

Green synthesis utilizes biological substances, such as extracts from plants, to assist in the production of nanoparticles. The process greatly decreases the requirement for noxious chemicals often employed in conventional chemical synthesis, therefore lowering environmental contamination and health hazards linked to the disposal of dangerous waste. The biological process is typically more cost-effective than conventional procedures, which employ easily accessible plant components that can be gathered in a sustainable manner, thereby decreasing the overall costs associated with nanoparticle manufacturing. This is especially beneficial for large-scale applications where affordability is essential. Biological techniques are frequently uncomplicated and can be carried out in gentle settings, such as at room temperature and with a neutral pH. The simplicity of the method not only increases its accessibility but also improves its ability to replicate nanoparticle manufacturing (Pal et al., 2022).

Cosmos caudatus, a botanical renowned for its therapeutic attributes, is used in harmony with the tenets of green chemistry, which advocate for safer and more sustainable methodologies in the field of nanotechnology. The biological constituents in *Cosmos caudatus* possess a high level of efficacy in reducing metal ions to nanoparticles, thereby optimizing the manufacturing process. *Cosmos caudatus* has a diverse range of phytochemicals, such as flavonoids, terpenoids, and phenolic compounds. These substances can reduce and stabilize nanoparticles during

their formation. The chemicals not only aid in the complexing of metal ions but also offer added advantages, such as improving the stability and biocompatibility of the produced nanoparticles. The antioxidant capabilities of *Cosmos caudatus* can enhance the stability and usefulness of the produced nanoparticles. In biomedical applications, the antioxidant activity of nanoparticles can play a crucial role in improving the effectiveness of therapy and minimizing the harmful effects on cells (Sarma et al., 2017). Nanoparticles produced by *Cosmos caudatus* have versatile applications across multiple domains, such as medicine (for the purpose of delivering drugs or acting as antimicrobial agents), agriculture (as environmentally friendly pesticides), and environmental remediation (to facilitate the breakdown of pollutants). The plant's versatility makes it an ideal choice for green synthesis methods that aim to produce nanomaterials with several functions.

Cosmos caudatus is a plant with phytochemical compounds that have not been explored before for ZnO NPs production. Azwanida et al., (2020) discovered that *Cosmos caudatus* has antimicrobial, antioxidant, antidiabetic, antifungal, anti-inflammatory, antihypertensive, and osteoprotective properties. The present activity pertains to the phytochemical composition of *Cosmos caudatus*, encompassing genistin, gentiatibetine, quercetin, phenyl propionic acid, orexin B, δ -humulene, stearidonic acid, and phenyl propionic acid (Firdaus et al., 2021). Phytochemical compounds possess reductive properties, enabling their use as reductants for zinc ions throughout the ZnO NPs' production. In addition, these compounds act as stabilizers and agents for capping in this process.

Cosmos caudatus thrives in tropical climates with 1,500–2,500 mm of annual precipitation. Fertile soil with a high organic content, thick texture, and good drainage can support plant growth on a wide range of soil types. A crop with a short growth cycle typically requires 3–4 months from the time of sowing to the final harvest. Leveraging rainfall patterns in the planted area requires proper planting timing. Tropical and subtropical areas, particularly in Southeast Asia, predominantly grow *Cosmos caudatus*. Key plantation regions include Singapore, Thailand, Indonesia, and Malaysia. It is extensively cultivated for culinary purposes in both rural and urban areas. Gardeners and small farmers grow it for local cuisine and medicine. *Cosmos caudatus* is a frequently available ingredient in local markets and a fundamental component of traditional cuisine in countries such as Malaysia and Indonesia. The demand is consistent because of its widespread popularity as both a salad element and an herbal treatment. Due to the rising knowledge of its health benefits, there is a growing interest in *Cosmos caudatus* in the health and wellness sector. The product comes in fresh leaves, dried powders, and supplements. There is potential for exporting *Cosmos caudatus* to regions outside of Southeast Asia, particularly those with a demand for unique and nutritious food options. Nevertheless, this industry is still in the process of growing and necessitates additional efforts in terms of promotion and

standards (Amin and Noor, 2014).

This study aimed to probe physiological, chemical, morphological, optical, and antimicrobial performance of ZnO NPs produced by using *Cosmos caudatus* leaf extract and zinc acetate precursors. Moreover, molecular docking was conducted to understand the way ZnO NPs interacted with proteins within three distinct microbial species.

2. MATERIALS AND METHODS

2.1 Chemical Reagents

In this work, the synthesis of ZnO NPs used zinc acetate dihydrate $Zn(CH_3COOH)_2 \cdot 2H_2O$ obtained from Merck and dried leaves of *Cosmos caudatus* from the region Gunung Pati Semarang central Java. Antimicrobial activity was analyzed using nutrient agar (Merck), potato dextrose agar (Merck), *Escherichia coli* (E. coli) strain ATCC 25922, *Staphylococcus aureus* (S. aureus) ATCC 25923, and *Aspergillus niger* ATCC 16404 at a concentration of 10^5 CFU/ml. Fluconazole and neomycin (100 mg/ml) were used as sequential positive controls for fungal and bacterial infections, respectively. All solutions were prepared using distilled water as the solvent.

2.2 Production of ZnO NPs

The scheme started with the generation of leaf extracts. Leaves were washed with water and then dried for 4 hrs in a dehydrator at 45°C. A mixture of 40 g desiccated leaves and 400 mL of water was heated at 50°C for 4 hrs. The mixture was subsequently subjected to filtration and extraction to obtain a plant extract. An examination of the compound in plant extract was performed using liquid chromatography-high resolution mass spectrometry (LC-HRMS) employing the UHPLC Vanquish Tandem Q Exactive Plus Orbitrap HRMS system manufactured by Thermo Scientific. Two grams of hydrated zinc acetate precursor ($Zn[CH_3COO]_2 \cdot 2H_2O$) were combined with 10 ml of *Cosmos caudatus* leaf extract, and the mixture was heated at 75°C, pH 6 into a paste-like consistency for 60 mins. After the formation of paste, it underwent calcination in a furnace at 600°C. The calcined powder is rinsed with distilled water and then dehydrated in the oven at a temperature of 50°C for 4 hrs. The purified powders were further evaluated and characterized.

2.3 Characterization

The material was analyzed using four distinct equipment, namely, scanning electron microscopy (SEM), X-ray diffraction (XRD), Fourier transform infrared spectroscopy (FTIR), and ultraviolet-visible spectroscopy. XRD was used to analyze the crystal structures using a Bruker AXS D8 Advance X-ray diffraction system at 40 kV voltage and 30 mA current with Cu K radiation (1.541) between 2θ 70°–80° angles. XRD data were validated using the JCPDS ZnO standard number 36–451. The average size of the crystallite was approximated by applying the Debye-Scherrer equation:

$$D = K \lambda / B \cos \theta \quad (1)$$

Where D and K are the average crystalline size and shape factors, respectively ($K = 0.9$), λ is the wavelength of the X-ray radiation ($\lambda = 1.54 \text{ \AA}$) for $K\alpha$ -Cu. θ and B represent Bragg's angle of diffraction and, respectively, the line width at half-maximal height.

FTIR spectroscopy (Bruker Tensor 27) operating within the wavenumber range $500\text{--}4000 \text{ cm}^{-1}$. The samples were then incorporated into KBr pellets for analysis. For absorbance measurement, a quantity of 0.01 g of ZnO NPs powder was evenly distributed within 20 mL of deionized water. The dispersion was scanned using a UV-Vis spectrophotometer (UV1800-Shimadzu) with a dual beam functioning at a precision of 1 nm within a working spectral spectrum of $200\text{--}500 \text{ nm}$.

2.4 The Assessment of Antimicrobial Effectiveness

The agar-well diffusion was employed to ascertain the antimicrobial activity (Daoud et al., 2019). A sterile medium consisting of potato dextrose agar (PDA) and nutrient agar (NA) was prepared on the petri dish. Fungi were cultured on PDA, while bacteria were grown on NA. A volume of 1 mL of either bacterial or fungal culture with a concentration of 10^5 CFU/mL was carefully transferred using a pipette and sprayed at the surface of a sterile petri dish. After solidifying, an aseptic cork borer sized 6 mm in diameter was used to cut a hole in the centre of the petri dish. Subsequently, two drops of a solution containing ZnO NPs at a 100 mg/mL concentration were introduced into the hole. The petri dish was then incubated at 37°C for 24 hrs to facilitate the growth of bacteria, whereas for fungi, the incubation period was extended to 5 days .

2.5 Molecular Docking

Interactions between two molecules, namely proteins and ZnO NP-ligands, were analyzed using molecular docking studies. Molecular docking is pivotal for understanding an inhibitor molecule's interactions with a target protein. Molecular docking studies were conducted using AutoDock-vina software. ZnO NPs have three dimensions, as acquired from the PubChem database. Protein molecules were determined using the Protein Data Bank (PDB). The simulation used proteins from the three types of microbes. For *Staphylococcus aureus*-type microbes using the transport lipoprotein HtsA (3EIX). HtsA plays a vital role in the transport of staphyloferrin A, a high-affinity iron chelator produced by *S. aureus*. In situations where iron is scarce, the Hts transporter system is very important for taking in iron-siderophore complexes, which are needed for bacteria to grow and stay alive. The growth of *S. aureus* in the presence of heme is not dramatically affected by the deletion of HtsA, according to research, which suggests that other routes may compensate for heme acquisition in the absence of HtsA (Beasley et al., 2009). *Escherichia coli* uses beta-ketoacyl-ACP synthase III (FabH) (1HNH), which is an enzyme with an essential function in the

synthesis of fatty acids. β -Ketoacyl-acyl-carrier-protein synthase III (FabH) is a crucial enzyme that plays a vital role in both the starting and extending stages of fatty acid production in bacteria and plants. The enzyme facilitates the first condensation step by incorporating two carbon atoms from malonyl-ACP into an acyl acceptor. Given its critical role in the manufacture of bacterial fatty acids, FabH is a highly desirable candidate for antibiotic development. Inhibition tactics encompass techniques such as competitively displacing substrates or disrupting the catalytic site (Qiu et al., 2001). Feruloyl esterase (1UWC) from *Aspergillus niger*. The Feruloyl Esterase (1UWC) enzyme derived from *Aspergillus niger* has a crucial function in the breakdown of hemicellulosic substances, which are important components of plant cell walls. This enzyme speeds up the breaking down of feruloyl-arabinose ester links in arabinoxylans, which are important parts of plant cell walls.

Feruloyl esterase is essential for the degradation of these intricate polysaccharides, enabling the fungus to use ferulic acid and other hydroxycinnamic acids as carbon sources (McAuley et al., 2004). The process of docking is accomplished through the preparation of the target and ligand structures by obtaining the three-dimensional (3D) structure of the target protein from databases such as the PDB. Ligand structure preparation includes steps defining the 3D conformations, protonation states, and assigning partial charges. Active site determination by identifying the binding site through analysis using computational tools that predict potential binding pockets. The Docking process involves generating possible conformations (poses) of the ligand within the binding site. Once potential poses are generated, a scoring function evaluates the binding affinity of each conformation. The top-ranked conformations are visualized using molecular visualization on the Protein Ligan Interaction Profiler web server. <https://plip-tool.biotech.tu-dresden.de/lip-web/plip/index> to analyze interactions such as hydrogen bonds, hydrophobic interactions, and electrostatic interactions, which contribute to binding affinity.

Experimental data on antimicrobial activity was employed to validate the simulation results. The docking results for the selected compound had the lowest energy. Binding energy is a vital quantity in molecular docking research since it measures the intensity of the interaction between a protein and its ligand. A lower binding energy signifies a more potent interaction, typically linked to increased effectiveness in drug or ligand activity. Studies have demonstrated that analysing the binding energies between ligands and microbial proteins might provide valuable information about their potential as candidates for ligands or drugs. The binding energy serves as an indicator of both the stability of the ligand-protein complex and the underlying molecular interactions. Interaction analysis could guide changes to increase binding affinity or specificity by identifying important protein residues that are essential for ligand binding (Adasme et al., 2021).

3. RESULTS AND DISCUSSION

3.1 Phytochemistry of *Cosmos caudatus* Leaf Extract

In the current study, a secondary metabolite found in the leaves of *Cosmos caudatus* was used to synthesize ZnO NPs. Secondary metabolites are chemical substances that plants

exude but are not directly involved in an organism's typical growth, development, or reproduction. The biologically active secondary metabolites are phytochemicals. The results of leaf extraction were analyzed using LC-HRMS to determine the phytochemical composition of the leaves used to reduce precursors in the production of ZnO NPs. A total of 39 phytochemical compounds were identified (Table 1).

Table 1. Compounds identified in *Cosmos caudatus* leaf water extracts analyzed Using Liquid chromatography-high resolution mass spectrometry (LC-HRMS)

| No | Compound | Molecular formula | Retention time (min) |
|----|--|--|----------------------|
| 1 | DL-Malic acid | C ₄ H ₆ O ₅ | 1.182 |
| 2 | D-(-)-Quinic acid | C ₇ H ₁₂ O ₆ | 1.126 |
| 3 | Methylmalonic acid | C ₄ H ₆ O ₄ | 1.666 |
| 4 | Citric acid | C ₆ H ₈ O ₇ | 1.448 |
| 5 | Astragalin | C ₂₁ H ₂₀ O ₁₁ | 9.464 |
| 6 | Corchori fatty acid F | C ₁₈ H ₃₂ O ₅ | 12.412 |
| 7 | 3,4,5-trihydroxy cyclo hex-1-ene-1-carboxylic acid | C ₇ H ₁₀ O ₅ | 1.28 |
| 8 | Salicylic acid | C ₇ H ₆ O ₃ | 10.007 |
| 9 | Fumaric acid | C ₄ H ₄ O ₄ | 1.206 |
| 10 | 1-O-acetyl-alpha-maltose | C ₁₄ H ₂₄ O ₁₂ | 1.12 |
| 11 | Gentisic acid | C ₇ H ₆ O ₄ | 4.226 |
| 12 | 2-C-methylerythritol 4-phosphate | C ₅ H ₁₃ O ₇ P | 1.073 |
| 13 | Diethylpyrocarbonate | C ₆ H ₁₀ O ₅ | 1.776 |
| 14 | (15Z)-9,12,13-Trihydroxy-15-octadecenoic acid | C ₁₈ H ₃₄ O ₅ | 13.113 |
| 15 | Picrocrocin | C ₁₆ H ₂₆ O ₇ | 10.353 |
| 16 | Dehydroascorbic acid | C ₆ H ₆ O ₆ | 1.49 |
| 17 | (-)-3-dehydroshikimic acid | C ₇ H ₈ O ₅ | 1.192 |
| 18 | 6-Hydroxy-5-methyl-4,11-dioxoundecanoic acid | C ₁₂ H ₂₀ O ₅ | 9.859 |
| 19 | (-)-3-dehydroshikimic acid | C ₇ H ₈ O ₅ | 1.457 |
| 20 | 4-Oxoproline | C ₅ H ₇ N O ₃ | 1.475 |
| 21 | Arabic acid | C ₅ H ₁₀ O ₆ | 1.125 |
| 22 | 1,2,3-cyclopropanetricarboxylic acid | C ₆ H ₆ O ₆ | 1.174 |
| 23 | 1-(2-Deoxy-5-O-phosphono-beta-D-erythro-pentofuranosyl)-1,2-dihydropyrimidine | C ₉ H ₁₅ N ₂ O ₆ P | 2.699 |
| 24 | Butopyronoxyl | C ₁₂ H ₁₈ O ₄ | 11.81 |
| 25 | D-(+)-Galactose | C ₆ H ₁₂ O ₆ | 1.134 |
| 26 | Hept-2-ulose | C ₇ H ₁₄ O ₇ | 1.153 |
| 27 | Uracil | C ₄ H ₄ N ₂ O ₂ | 1.468 |
| 28 | 1-O-Arsonopentofuranose | C ₅ H ₁₁ As O ₈ | 0.978 |
| 29 | 2,3-Dihydro-1-benzofuran-2-carboxylic acid | C ₉ H ₈ O ₃ | 8.203 |
| 30 | 10,16-Dihydroxyhexadecanoic acid | C ₁₆ H ₃₂ O ₄ | 13.624 |
| 31 | 2-[3,8-Dihydroxy-8-(hydroxymethyl)-3-methyl-2-oxodecahydro-5-azulenyl]-2-propanil hexopyranoside | C ₂₁ H ₃₆ O ₁₀ | 11.028 |
| 32 | 4-Hydroxy-L-threonine | C ₄ H ₉ N O ₄ | 1.47 |
| 33 | (-)-Threo-isodihomocitric acid | C ₈ H ₁₂ O ₇ | 1.261 |
| 34 | 2-Oxoglutaric acid | C ₅ H ₆ O ₅ | 1.19 |
| 35 | Diethylpyrocarbonate | C ₆ H ₁₀ O ₅ | 1.54 |
| 36 | 4-Oxoproline | C ₅ H ₇ N O ₃ | 1.208 |
| 37 | 4-Indolecarbaldehyde | C ₉ H ₇ N O | 9.473 |
| 38 | Indole-3-acetic acid | C ₁₀ H ₉ N O ₂ | 8.562 |
| 39 | Benzoic acid | C ₇ H ₆ O ₂ | 7.13 |

Carbohydrates, carboxylic acids, flavonoids, alkaloids, and amino acids were among the extracted compounds. These compounds include vitamins, fatty acids, alcohols, polyphenols, ketones, hydroxybenzoic acid, and aldehydes.

Firdaus et al. (2021) extracted *Cosmos caudatus* leaves using maceration with hot water solvents. The LCMS/MS test identified 12 bioactive chemicals. There were genistin, gentiabin, quercetin, oroxin B, ε-humulene, stearidonic acid, phenylpropionic acid, and spathulenol in the leaf extract. Azwanida et al. (2020) prepared the *Cosmos caudatus* leaf extract by immersing it in boiling water at room temperature for a duration of 30 minutes. LC-UV-MS/MS study of the extracts indicated the presence of up to 22 chemicals. The extraction findings by Noriham et al. (2015) demonstrate the impact of both solvent type and leaf maturity rate (young, mature, and old). HPLC analysis detected and identified a total of 12 chemicals. The compounds include caffeic acid, gallic acid, vanillic acid, chlorogenic acids, p-coumaric acid, synapic acid, quercetin, myricetin, ferullic acid, rutin, epicatechin, and catechin. The recent research employed distilled water as a solvent, maintaining a precisely controlled for 4 hrs at 50°C. The resultant extract was found to contain a total of 39 bioactive components. Compared to prior investigations, the experiment yielded a greater quantity of chemicals. Prolonged extraction durations and elevated temperatures are responsible for the quantity of chemical yield. Increasing the duration of the extraction process enhances the likelihood of extracting a greater quantity of bioactive chemicals.

Plants contain diverse reductive antioxidants, including alkaloids, polysaccharides, flavonoids, saponins, polyphenols, vitamins, amino acids, tannins, and terpenoids.

Plant extracts are reducing agents and reactants for zinc salt solutions that are used to synthesize zinc oxide nanoparticles. This study evaluated the chemical composition of *Cosmos caudatus* extract, revealing the presence of numerous components capable of functioning as reducing agents. These reducing agents facilitate the transformation of precursors to zinc oxide with enhanced efficiency. In the presence of ascorbic acid, the precursors underwent dissociation, producing Zn²⁺ ions in the solution. Simultaneously, the L-ascorbic acid contained within the leaf extract undergoes oxidation, forming L-dehydroascorbic acid through free radical mechanisms.

ZnO NPs are synthesized through a calcination process, which exposes the precursor material to high temperatures. Visveshwari et al., (2017) demonstrated that phenolic compounds, which include hydroxyl functional groups, can form bonds with Zn²⁺ ions, leading towards formation of the Zn(OH)₂. Subsequently, these compounds can undergo calcination in muffle furnaces at temperatures exceeding 400°C to synthesize ZnO NPs. In a study by the Osuntokun et al., (2019), It was noticed that metal ions can form enduring complexes with aromatic hydroxyl groups. Mayedwa et al., (2018) presented a research report outlining a mechanism for producing ZnO NPs, drawing upon data from previous research. The creation process is delineated by the mechanism shown in Fig. 1.

Fig. 1 illustrates the molecular structure of several bioactive compounds found in the leaf extract of *Cosmos caudatus*, as well as the reaction mechanisms involving one of the constituents of gentisic acid. The proposed reaction mechanism demonstrates that *Cosmos caudatus* leaf extract converts precursors into ZnO NPs. Zinc ions bind to aromatic hydroxyl groups, forming stable complexes containing zinc and gentisic acid. Following the annealing process, the complex disintegrates, forming ZnO NPs.

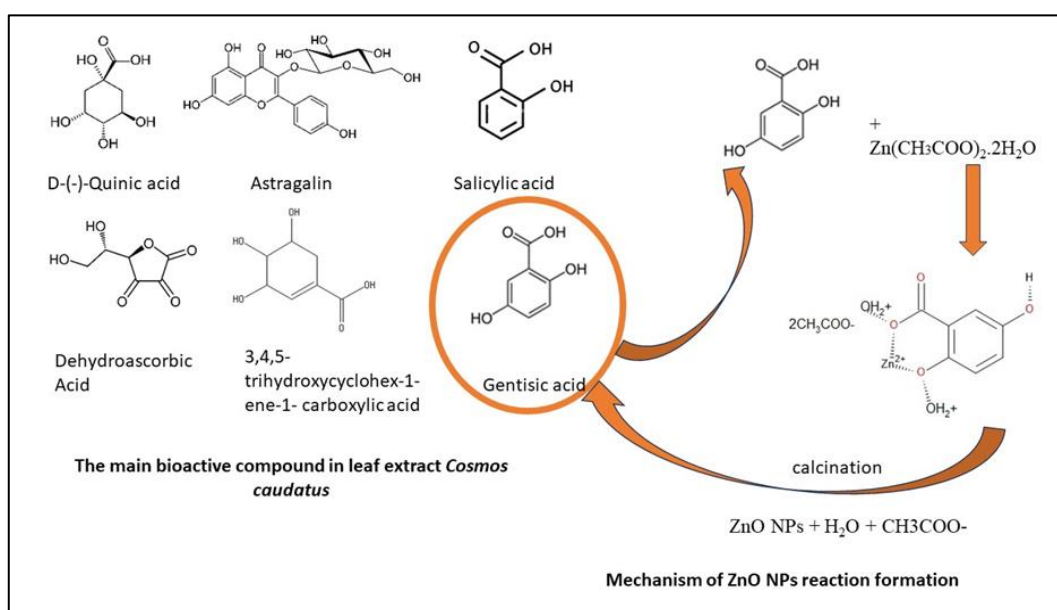


Fig. 1. The proposed mechanism of the formation reaction of ZnO NPs with the gentisic acid compounds present in the

Cosmos caudatus leaves extract

(Hajiashrafi and Motakef-Kazemi, 2018).

Compounds containing the aromatic hydroxyl group are accountable for complex formation. The existence of a carboxylate cluster enhances the stability of the ZnO NPs and inhibits their development (Mayedwa et al., 2018). Because zinc ions are bonded to aromatic hydroxyl clusters, a stable complex forms between zinc and gentisic acid 1. Complicated annealing processes produce ZnO NPs. D-(-) quinic acid, astragalin, salicylic acid, dehydroascorbic acid, gentisic acid, DL malic acid, 1-O-acetyl-alpha-maltose, 2-C-methylerythritol 4-phosphate, picrocrocin, citric acid, the (-)-3-dehydroshikimic acid, arabic acid, hept-2-ulose, and 1-o-Arsonopentofuranose are some of the chemicals that are found in *Cosmos caudatus* extracts. The chemicals have aromatic hydroxyl groups that can combine with Zn^{2+} ions from the precursor.

Previous studies, by Barzinjy et al. (2018), have presented a mechanism for the creation of ZnO NPs by reducing them with plant extracts. The study's findings reveal a three-stage process that forms ZnO NPs. Firstly, nucleation occurs, followed by the absorption of Zn ions on the surface of biomolecules. Plant compounds then reduce the absorbed ions to form the nanophase. The growth mechanism then forms nanolayers, leading to the mass production of Zn nanostructures. Annealing at approximately 500°C, the final stage, oxidizes the ZnO mass and produces crystalline structures. Ansari et al. (2020) state that eugenol, a capping agent present in plant extracts from *Cinnamomum verum*, forms ZnO NPs. Zinc ions (Zn^{2+}) will combine with the phytochemical found in plant extracts to create ZnO NPs. The process of synthesizing ZnO NPs from *Cayratia pedate* extract consists of three stages: activation (including reduction of metal ions and formation of reduced metal ion nuclei), growth (resulting in the development of stable nanoparticles), and termination (leading to the final generation of nanoparticles) (Jayachandran et al., 2021). *Ficus carica* leaf extracts contain botanical chemicals including phenolic substances, organic acids, alkaloids, and flavonoids, which work as both reducing and capping agents. Electrostatic attraction causes ZnO NPs that are next to each other to interact, which forms ZnO clusters (Arumugam et al., 2021).

3.2 Structure of ZnO Particle Nanocrystals

Synthesized from *Cosmos caudatus*

XRD analysis was performed at angles of 20°–70° to confirm the growth of ZnO NPs. The results of the analysis are shown in Fig. 2, demonstrating peaks at 34.42°, 36.35°, 37.44°, 47.54°, 56.60°, 62.86°, 66.38°, 67.96°, and 69.10°. The diffraction pattern in the image was matched by the Joint Committee on Powder Diffraction Standards number 36–1451 for ZnO with a hexagonal wurtzite crystal phase with a grid constant (lattice) of $a = b = 0.32$ nm and $c = 0.52$ nm. No additional peaks in the XRD pattern confirmed that the generated ZnO NPs were pure. The presence of a distinct and slender peak in the XRD spectrum indicates that zinc oxide exhibits a well-defined crystalline structure

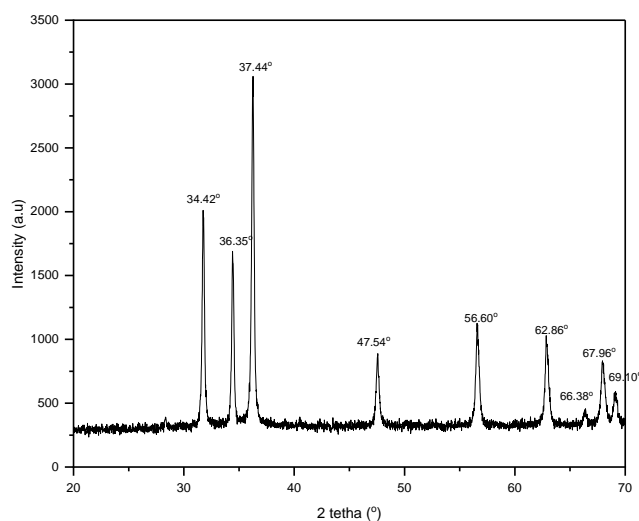


Fig. 2. Analysis of XRD ZnO NP green synthesis results with the leaf extract *Cosmos caudatus*

The diameter of the crystal was 50.54 nm according to the Debye-Scherrer equation. The formation of ZnO NPs affected the size and diameter of the formed crystals. The sol-gel synthesis method produced a ZnO crystal size of 31.3 nm possessing a d-spacing between planes of 0.2472 nm (Limón-Rocha et al., 2022). In comparison, synthesizing nanoparticles through wet chemicals results in a crystalline diameter of 31.86 nm and a structured crystal with a wurtzite lattice and defined grid parameters ($a = 0.32$ nm and $c = 0.56$ nm) (Hajiashrafi and Motakef-Kazemi, 2018). Mayekar et al., (2014) synthesized ZnO NPs using a thermal decomposition method to obtain a crystalline size of 39.91 nm.

Acalypha indica leaf extract allied to zinc acetate precursor results in the synthesis of ZnO NPs measuring 16 nm in diameter, exhibiting a high level of purity (Kamarajan et al., 2022). Greeshma and Thamizselvi (2022) add leaf extracts of *Catharanthus roseus* and *Morinda citrifolia* to form ZnO NPs with a crystallite size of 17.44 nm. Various factors influence the disparity in crystal sizes. One example is the composition of bioactive compounds in leaf extracts. Various plant species synthesize distinct phytochemical substances. These phytochemical compounds' function groups engage with both the creation and stability of nanoparticles. Furthermore, polyols, including terpenoids, flavons, and polysaccharides, possess the capacity to reduce the concentration of metal ions during the growth of nanoparticles (Vasquez et al., 2016). Hence, the composition and dimensions of the ZnO NPs vary based on the specific plant species employed.

3.3 Analysis of Functional Groups Using FTIR

FTIR spectrum in Fig. 3 exhibits a prominent peak at a wavenumber of 405.94 cm^{-1} , indicating Zn-O stretching

(Nandiyanto et al., 2019). The peak noted at a wavelength of 875.84 cm^{-1} corresponds to the vibrational mode associated with C-O stretching. The predominance of a peak at 1043 cm^{-1} indicates a C-O stretch. The observed peaks at a wavenumber of 1437.48 cm^{-1} are attributable to C-H bending vibrations in alkanes. According to Sangeetha et al. (2011), the Zn-O peak region of the vibration mode is situated within the wavelength range of 600 cm^{-1} to 400 cm^{-1} . The peak observed at 3421 cm^{-1} indicates O-H stretching groups, which are commonly found in many compounds such as carboxylic acids, polyphenols, flavonoids, and alkaloids (Visveshwari et al., 2018). The observed changes in the position and intensity of the spectrum of the sample can be ascribed to the interaction between the flavonoid and functional phenol groups with the ZnO NPs (Awasthi et al., 2015).

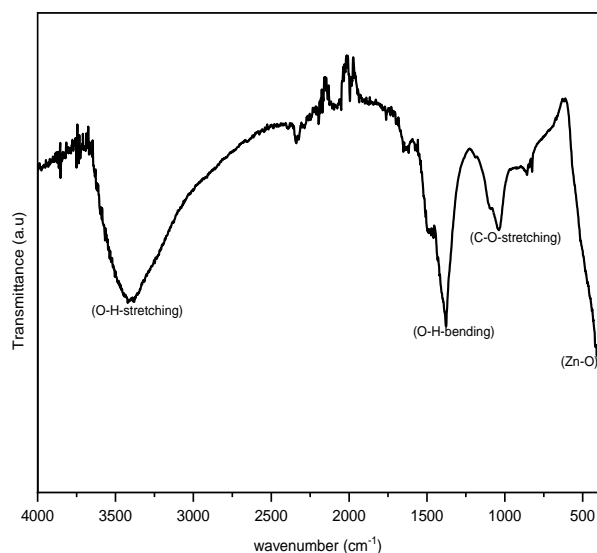


Fig. 3. Analysis of FTIR ZnO NPs green synthesis results with the leaf extract *Cosmos caudatus*

Ocimum sanctum leaf extract and zinc acetate precursor are utilized in the growth of ZnO NPs. The primary absorption peaks of nanoparticles synthesized are $3450\text{--}3350$, $2950\text{--}2900$, $2450\text{--}2350$, $1450\text{--}1400$, and $500\text{--}400\text{ cm}^{-1}$. A wide peak at $3450\text{--}3350\text{ cm}^{-1}$ is due to the vibration of tension between O and H that is present in phenolic and carboxylic acids. In the O-H group, alkylated peaks are at $2450\text{--}2350\text{ cm}^{-1}$. As for N-O stretching in the nitro group, a sharp peak is observed at $1450\text{--}1400\text{ cm}^{-1}$. Each sample showed an intense bandwidth within the spectrum of $500\text{--}400\text{ cm}^{-1}$ due to the vibrational properties of the ZnO nanocrystal. Phytochemical compounds convert nitrate ions from precursors into oxides. Peak wave numbers of the 2974.25 cm^{-1} and 1437.04 cm^{-1} indicate the presence of flavonoid and phenolic molecules in leaf extracts and confirm phytochemistry. During the formation of nanoparticles, plant material's phytochemistry acts as a reduction substance (Kamarajan et al., 2022).

3.4 Morphological Analysis

Fig. 4 depicts a 30,000-fold magnification of the SEM image of the ZnO NPs. The image displays ZnO NPs with a consistent hexagonal shape and a relatively small diameter. The particle morphology often exhibits a hexagonal shape, which is characterized by a consistent diameter. The composition of polyphenol compounds in each extract determines the morphology, dimensions, and spatial arrangement of the NPs produced through the complex formation pathway, which alters the nucleation and growth mechanisms of ZnO NPs (Zhu et al., 2021). Particle aggregation at the surface is evident from the elevated surface energy inherent to the nanoparticle synthesis (Roxy et al., 2021).

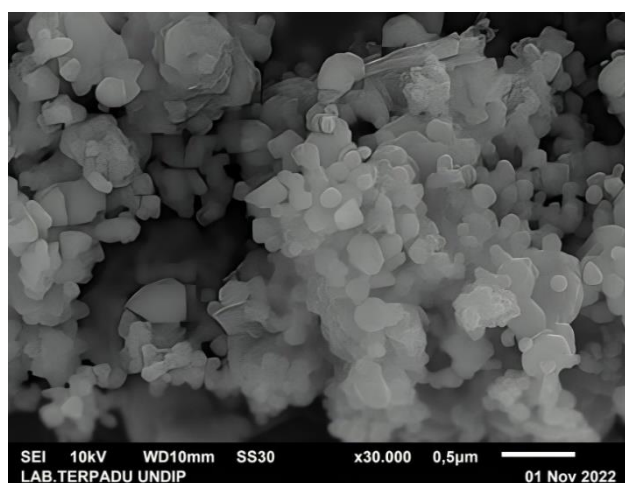


Fig. 4. Morphological analysis of ZnO NPs green synthesis results with leaf extract *Cosmos caudatus*

The biological method yields ZnO NPs with a smooth surface shape and a tiny size when calcinated at a temperature of 400°C (Kamarajan et al., 2022). Nizamuddin et al., (2022) reported that an extract from the leaves of the *Carica papaya*, which is in the Caricaceae family, can make ZnO NPs with a hexagonal bone shape and a size of less than 50 nm . *Acalypha fruticosa* L. leaf extract produces ZnO NPs with a consistent, non-aggregated, and evenly distributed spherical shape. The mean particle size recorded is 55 nm (Vijayakumar et al., 2020). The use of a Swertia chirayitac stem extract in ZnO synthesis results in the formation of a spherical crystalline structure with a minimum size of 17 nm (Saha et al., 2021). ZnO NPs of sizes 25 to 70 nanometers are made by *Passiflora caerulea*, *Sambucus ebulus*, *Peganum harmala*, and *Crocus sativus*. The extract from the *Hibiscus subdariffa* flower produces zinc oxide nanoparticles that resemble the shape of a cabbage flower, with an average diameter of 300 to 400 nm . Instead, the extract from *Veronica multifidi* makes nanoparticles that are almost spherical and hexagonal, with average diameters between 10 nm and 100 nm (Rajendrachari et al., 2021). The *Cucurbita* seed extract forms hexagonal particles with minimal aggregation. The

produced ZnO NPs vary in size from 45 to 90 nm. The ZnO NPs that were produced have enormous dimensions due to their tendency to form aggregates despite their initial tiny size. The HRTEM study showed clear black and white areas, which shows that ZnO has properties that make it both hydrophilic and hydrophobic (Velsankar et al., 2019). The *Garcinia Cambogia* fruit pulp extract makes particles that are about the shape of a ball and are evenly spread out and clumped together. These particles are between 120 nm and 160 nm in size. Particle agglomeration occurs due to the polarity and of nanoparticles (Sasi et al., 2022). The existence of numerous polyphenol chemicals in each extract affects the mechanisms of nucleation and growth of ZnO NPs, determining their form, size, and distribution during the complex formation pathway synthesis (Nava et al., 2017).

3.5 Optical Properties

Fig. 5 depicts a monochromatic absorption measurement as a function of the wavelength above the ZnO UV spectrum of the NPs. A significant increase in absorption between 200nm and 400 nm indicates zinc oxide (Elbrolesy et al., 2023). Maximum absorbance values were achieved at a wavelength of 385 nm. These absorption results demonstrate a red shift and the bandgap energy declining. Inset of Fig. 5 shows the Tauc absorbance plot of the ZnO NPs. The measured band gap value was 3.04 eV. The calculation revealed an optical band gap red shift with a magnitude of 3.04 eV compared with the energy gap band value of 3.37 eV observed in the ZnO bulk material.

Zinc oxide is a direct-bandgap semiconductor. Determining the bandgap energy entails the use of the Tauc

plot, which involves plotting the absorption energy values. The Tauc plot demonstrates that the strength of optical absorption is contingent upon the disparity between the photon energy and the band gap, as denoted by Eq. (2):

$$(\alpha h\nu)^{1/n} = A^*(h\nu - E_g) \quad (2)$$

The symbols used in this text correspond to several physical quantities. Specifically, h represents Planck's constant, ν denotes the frequency of a photon, α reflects the absorbance coefficient, E_g refers to the bandgap, and A^* signifies the slope of a plot in the Tauc analysis inside a linear region. The number of energy levels corresponds to the propensity of electron transitions, with $n = 1/2$ denoting direct and two denoting indirect transitions.

The results of UV-vis spectroscopy analyses of ZnO NPs synthesized via reduction with the aid of chemicals in plant extracts will exhibit variability. According to Nilavukkarasi et al. in 2020, the nanoparticle made from *Capparis zeylanica* leaf extract revealed a band gap of 3.68 eV and its peak absorption is at 356 nm in the UV-visible spectrum. In contrast, Chakraborty et al. (2020) reported that *Averrhoa carambola* fruit extract ZnO NPs exhibit significant absorptions at 350 nm wavelengths and 3.2 eV band gap energy. *Saffron* corm extract produces ZnO NPs with an energy gap of 3.37 eV and a peak absorbance characteristic of 368 nm (Owais Mushtaq et al., 2022).

The co-precipitation method synthesized ZnO NPs with a band gap energy of 3.03 eV and a peaking absorbance value of 409 nm. On the other hand, ZnO NPs synthesized through the sol-gel method exhibited a band gap energy of 3.13 eV and an absorbance of 395 nm (Kanwal et al., 2023). The band gap energy of ZnO NPs formed through hydrothermal approaches using $ZnSO_4$ solution as a

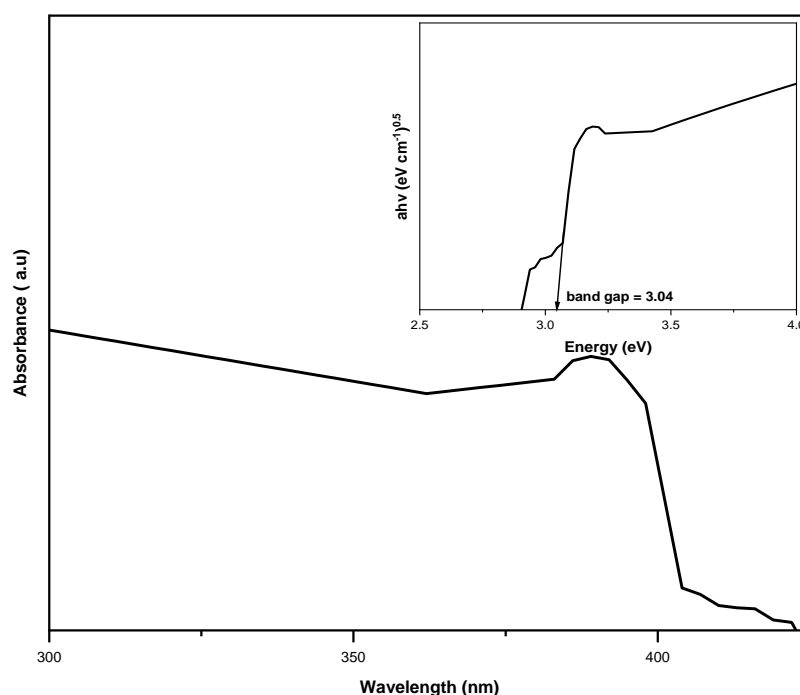


Fig. 5. Monochromatic UV-Vis absorption and Tauc plot ZnO NPs green synthesis results with the leaf extract *Cosmos*

precursor was estimated at around 3.18 eV (Saad et al., 2019). ZnO with a band gap value of 3.38 eV was synthesized from zinc nitrate hexahydrate precursor using the hydrothermal method (Shahat et al., 2022).

The band gap of ZnO NPs is a crucial factor affecting their optical and electronic characteristics, rendering them appropriate for various applications, including photocatalysis, sensors, and optoelectronic devices. The capacity to adjust the band gap in ZnO NPs has important consequences for various applications. ZnO NPs have a greater band gap and can effectively absorb UV light, which is useful for photocatalytic applications, such as breaking down organic contaminants. ZnO NPs have a heightened responsiveness to UV light and possess a changeable band gap, which can significantly improve the efficiency of gas sensors and biosensors. By manipulating doping and controlling the size, it becomes possible to customize the band gap, creating ZnO-based LEDs and laser diodes that function in the UV spectrum. The structure and morphology of the ZnO NPs absorption spectrum are highly contingent upon particle size, dielectric medium, and the surface-adsorbed species (Nagababu et al., 2018). The red shift is directly proportional to the particle size, quantum confinement effects, low-energy transition blockages, and surface morphological alterations. In addition, the absence of oxygen, dirt, and band gaps plays a crucial function in establishing sample absorption values (Agarwal et al., 2019).

3.6 Antimicrobial Activity

Fig. 6 depicts the antimicrobial activity of the ZnO NPs against three categories of microorganisms: *Staphylococcus aureus* (gram-positive), *Escherichia coli* (gram-negative), and *Aspergillus niger* (mold). A 100 mg/ml concentration of ZnO NPs induced distinct inhibition zones in various microorganisms. The inhibition zones for gram-positive *Staphylococcus aureus* and gram-negative *E. coli* were 5.38

caudatus

± 0.76 mm; for gram-negative *Escherichia coli*, it was 7.38 ± 0.92 mm; and for mold, it was 6.13 ± 0.74 mm. Owing to structural dissimilarities in the cell walls, gram-negative bacteria are more susceptible to growth inhibition. Using neomycin as a positive control led to an inhibitory zone of 50 ± 0.12 mm for *E. coli* and 43 ± 0.22 mm for *S. aureus*. In contrast, fluconazole exhibited a barrier zone of 34 ± 0.032 mm against *A. niger*.

Gram-positive bacteria possess a comparatively thick peptidoglycan coating, ranging in thickness from 20 to 80 nm, on their cellular walls. Gram-negative bacteria possess a comparatively weak peptidoglycan coating on their cell walls and an outer membrane composed of lipopolysaccharides. The peptidoglycan layer is composed of replicating units of amino acids and carbohydrates. ZnO NPs can form bonds with carboxylic acids and amino groups, thereby exhibiting inhibitory biological activity. This property enables ZnO NPs to readily permeate the peptidoglycan layer and damage gram-negative bacteria. In comparison to the gram-positive bacteria, and of the gram-negative bacteria are more susceptible to antimicrobial agents (Sasi et al., 2022).

ZnO NPs can dissolve in aqueous environments, releasing Zn^{2+} ions. These ions can adsorb onto the negatively charged surfaces of bacterial cells, disrupting their metabolic processes and inhibiting protein synthesis, ultimately leading to cell death. ZnO NPs can produce reactive oxygen species, especially under light irradiation. These reactive oxygen species (ROS) can cause oxidative stress in bacterial cells, damaging cellular components such as lipids, proteins, and DNA. The oxidative damage often results in cell membrane disruption and increased permeability, leading to cell lysis (Yang et al., 2023). The positive charge of ZnO NPs enhances their interaction with negatively charged bacterial membranes. This electrostatic attraction can facilitate the penetration of ZnO NPs into the

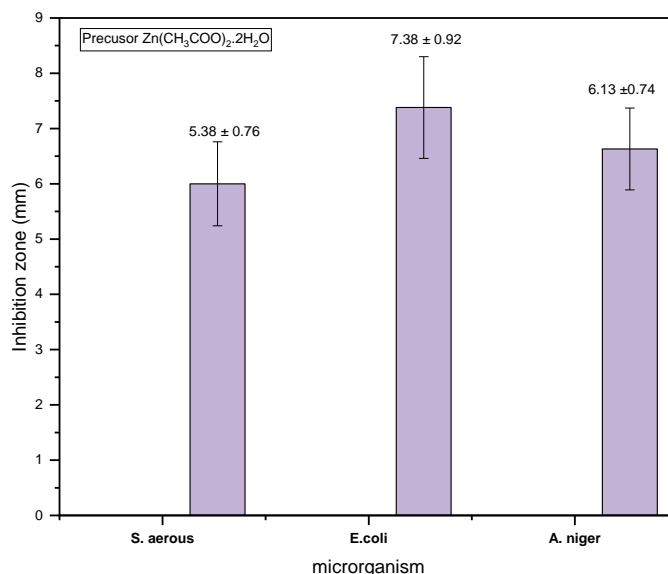


Fig. 6. Microbial inhibition zone green ZnO NPs synthesis with leaf extract of *Cosmos caudatus*

bacterial cell, causing structural damage and contributing to their antimicrobial activity (Mendez et al., 2022). Studies have shown that ZnO NPs can physically disrupt bacterial cell membranes. The nanoparticles can penetrate the membrane, leading to the formation of pores and subsequent leakage of cellular contents, which is detrimental to cell viability. The antibacterial efficacy of ZnO NPs is also influenced by their size and shape. Smaller nanoparticles and those with higher surface area-to-volume ratios tend to exhibit stronger antibacterial activity due to their enhanced reactivity and ability to penetrate bacterial cells more effectively (Babayevska et al., 2022).

Similar to their antibacterial action, ZnO NPs can disrupt the membranes of fungal cells. This disruption can lead to cell leakage and death, particularly in pathogenic fungi. ZnO NPs can interfere with the metabolic pathways of fungi, inhibiting their growth and reproduction. The release of Zn^{2+} ions play a crucial role in this inhibition, affecting enzyme activities necessary for fungal metabolism. Just as with bacteria, the generation of ROS in fungal cells can lead to oxidative stress, damaging cellular components and contributing to cell death. This mechanism is particularly effective against various fungal species, making ZnO NPs a potential antifungal agent (El-Fallal et al., 2023).

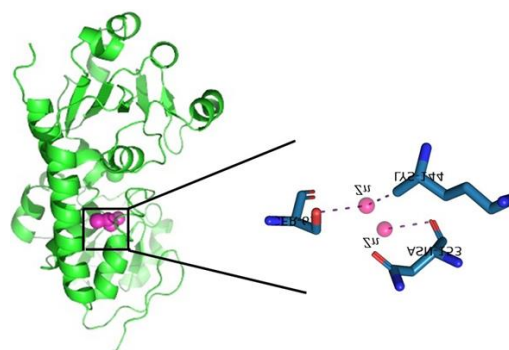
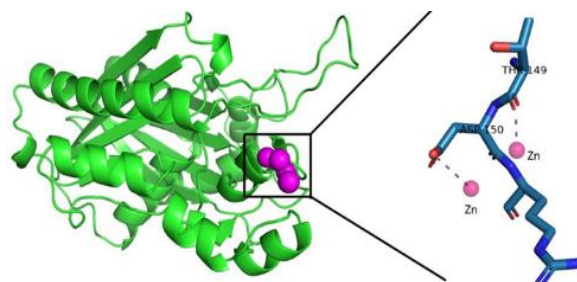
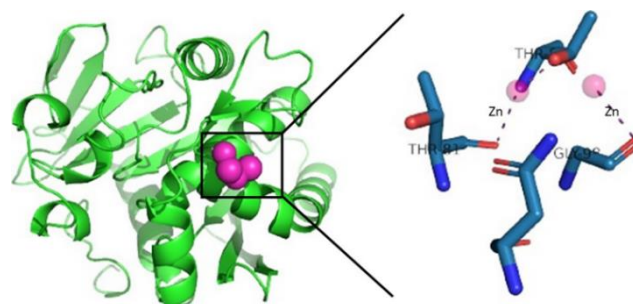
The results were identical in an antibacterial investigation using ZnO NPs from *Nilgiriantus ciliatus* leaf extract. The ZnO NPs inhibition zone of *Cosmos caudatus* exhibited lower values than NPs generated from *Euphorbia hirta* leaf extract (Resmi et al., 2021). The presence of a 100 mg/ml solution leads to the formation of an inhibition zone measuring 24 mm in diameter for *E. coli*, whereas for *A. niger*, the inhibition zone measures 20 mm in radius (Ahmad and Kalra, 2020).

3.7 Molecular Docking

Figs. 7, 8, and 9 depict the results of the docking study. Each figure shows the dynamic interplay between the protein and the ligand (ZnO NPs). *Staphylococcus aureus* HtsA (3EIX) transport lipoprotein interacts with ligand (ZnO NPs) with a binding energy of -2.3 kcal/mol. The interplay between *Escherichia coli* and *Aspergillus niger* results in successive binding energies of -3.4 kcal/mol and -2.6 kcal/mol. Reduced binding energy is associated with increased antibacterial efficacy (Aravin et al., 2022). The statement aligns with the available data from an antimicrobial probe. The docking results revealed that 2.56 hydrogen bonds were formed between oxygen and SER63A residues in *Staphylococcus aureus*, whereas ASN153A, SER63, and LYS 144A formed metal complexes with Zn at 2.53, 2.64, and 2.59, respectively. At 3.09 Angstroms, *Escherichia coli* exhibited interactions in the presence of hydrogen-binding residues in ARG151A. The THR149A and ASP150A residues exhibited metal complex formation with successions of 2.28 and 2.62, respectively. *A. niger* engages in interaction by establishing a hydrogen bond with

the ASN79A residue, which occurs at a distance of 2.11 units.

The GLY98A, THR81A, and THR83A residues also formed a metal complex with consecutive distances of 2.58, 2.45, and 2.36 units, respectively. The results of the docking analysis indicated a lack of contact between the tested compound and the amino acid residues containing sulfur, namely, methionine and cysteine. Sulfur atoms can undergo surface coverage, which renders them less prone to hydrogen bonding interactions (Prasad et al., 2020).

**Fig. 7.** ZnO NPs interaction with HtsA transport lipoprotein (3EIX) of *Staphylococcus aureus***Fig. 8.** ZnO NPs interaction with beta-ketoacyl-ACP synthase III (FabH) (1HNH) of *Escherichia coli***Fig. 9.** ZnO NP interaction with Feruloyl esterase (1UWC) of *Aspergillus niger*

Binding energy is a fundamental notion in biology, chemistry, and physics. It specifically refers to the amount of energy needed to separate a group of particles into individual components. This phenomenon's biological significance extends across multiple levels of organization,

encompassing molecular interactions, cellular structures, and beyond. Binding energy plays an important role in understanding chemical interactions at the molecular level, particularly in biological macromolecules such as proteins and nucleic acids. The energy associated with these chemical bonds impacts molecules stability and reactivity. For example, bond-dissociation energy, which quantifies the energy required to separate a chemical bond, is crucial in biological activities, particularly in enzyme-substrate interactions. Strong binding energies frequently correspond to stable interactions, essential for protein structural integrity and enzyme activity. Binding energies have a significant impact on protein folding and overall protein stability. The interplay among amino acids, including hydrogen bonding, ionic interactions, and van der Waals forces, collectively contributes to the total binding energy of a protein. A positive binding energy signifies a stable conformation essential for the optimal functioning of proteins in biological systems. Differences in binding energy can result in protein structure and function variations, which can impact activities such as signal transduction and metabolic pathways. The stability of DNA and RNA structures relies heavily on the binding energies present in nucleic acids. The binding energy generated by base pairing affects the melting temperature of nucleic acid duplexes, a critical factor in DNA replication and transcription. The interactions mentioned here play a crucial role in maintaining the stability of genetic information and ensuring the appropriate functioning of cells. Cellular recognition processes, such as receptor-ligand interactions, are similarly regulated by binding energies. The binding energies of these interactions determine the effectiveness of signaling pathways and the accuracy of molecular recognition (Boz and Stein, 2021).

Strains of *Escherichia coli* and *Staphylococcus epidermidis* are susceptible to ZnO NPs, as shown by molecular docking and antimicrobial performance analysis. The binding energy of -7.5 kcal/mol between TagF polymerases in *S. epidermidis* serves as a demonstration of this sensitivity. The interaction of ZnO NPs with AcrAB-To1C *E. coli* results in a binding energy of -7,36 Kcal/mol (Alvarez-Chimal et al., 2022). Different amino acid compositions of the targeted protein dependence the interaction of ZnO NPs with different types of microbes. The magnitude of the free-binding energy value and the type of amino acids each protein contains provide evidence for the interaction.

Utilizing plant extracts such as *Cosmos caudatus* to produce ZnO NPs offers an eco-friendly and economical substitute for chemical and physical techniques. Plant-based synthesis is more environmentally friendly, cost-effective, non-toxic, and compatible with living organisms than alternative processes. *Cosmos caudatus* is a readily accessible plant, making it an appropriate selection for the large-scale production of ZnO NPs. Plant extracts provide a cost-effective and environmentally advantageous substitute for employing intermediary base groups. The

phytochemicals found in *Cosmos caudatus*, including polyphenolic compounds, alkaloids, polysaccharides, amino acids, vitamins, and terpenoids, can function as both complexing and capping agents to stabilize throughout the biological process. These chemicals facilitate the creation and maintenance of ZnO NPs. ZnO NPs produced using *Cosmos caudatus* have demonstrated encouraging outcomes in several medicinal uses, including antibacterial, anti-cancer, anti-diabetic, and antioxidant properties.

The synthesis of ZnO NPs is achieved by using an extract obtained from the leaves of *Cosmos caudatus*. The study focuses on one sort of variable and investigates the antibacterial uses of the produced nanoparticles. The variables involved in the synthesis process will affect the physico-chemical properties of the resulting zinc oxide nanoparticles. This, in turn, can influence the effectiveness of these nanoparticles in a variety of application fields. Therefore, additional research is necessary regarding the numerous process variables, characteristics, and broader potential applications of this material.

4. CONCLUSION

Green synthesis using *Cosmos caudatus* leaf extract produces ZnO NPs with a 50.54 nm hexagonal crystal phase. While the observed morphology of ZnO NPs is hexagonal and their diameters are nearly uniform, the optical properties of zinc ZnO NPs exhibit a peak absorption at a wavelength of 385 nm, coupled by a band gap energy of 3.04 eV. A reduction agent of phytochemical compounds in leaf extracts with an OH functional group forms a complex with Zn²⁺ ions as part of the mechanism for the formation of nanoparticles. The magnitude of the binding energy acquired through molecular docking provides evidence for this observation.

DECLARATION OF COMPETING INTERESTS

The authors declare no conflict of interest.

ACKNOWLEDGMENT

This project was supported by the Educational Fund Management Institution (LPDP), Ministry of Finance, and the Directorate General of Higher Education, Research, and Technology of the Republic of Indonesia. Financial support was also provided by DRPM Kementerian Pendidikan, Kebudayaan, Riset dan Teknologi Indonesia (contract number 038/E5/PG.02.00.PL/2024 and 1763/PKS/ITS/2024 through the "Penelitian Fundamental Reguler" scheme. The authors also expressed their gratitude to the International Research Mobility ITS 2024.

REFERENCES

- Aabid, A.A., Humadi, J.I., Ahmed, G.S., Talib Arullah, A., Ahmed, M.A., Abdullah, W.S. 2023. Enhancement of desulfurization process for light gas oil using new zinc oxide loaded over alumina nano catalyst. *Applied Science and Engineering Progress*, 16, 6756–1804.
- Abdelhamid Shahat, M., Ahmed Ghitas, El-Hossary, F.M., Abd El-Rahman, A.M. 2022. ZnO nanoparticles for photocatalytic methyl orange degradation : hydrothermal synthesis , characterization , and optimization ZnO nanoparticles for photocatalytic methyl orange degradation. *Materials Science and Engineering*, 1269, 012010.
- Adasme, M.F., Linnemann, K.L., Bolz, S.N., Kaiser, F., Salentin, S., Haupt, V.J., Schroeder, M. 2021. Plip 2021: Expanding the scope of the protein-ligand interaction profiler to DNA and RNA. *Nucleic Acids Research*, 49, W530–534.
- Agarwal, H., Nakara, A., Shanmugam, V.K. 2019. Anti-inflammatory mechanism of various metal and metal oxide nanoparticles synthesized using plant extracts: A review. *Biomedicine and Pharmacotherapy*, 109, 2561–2572.
- Ahmad, W., Kalra, D. 2020. Green synthesis, characterization and anti microbial activities of ZnO nanoparticles using *Euphorbia hirta* leaf extract. *Journal of King Saud University–Science*, 32, 2358–2364.
- Alvarez-Chimal, R., Garcia-Perez, V.I , Alvarez-Pe´rez, M.A., Tavera-Hernandez, R., Reyes-Carmona, L., Martinez-Hernandez, M., Arenas-Alatorre, J.A. 2022. Influence of the particle size on the antibacterial activity of green synthesized zinc oxide nanoparticles using *Dysphania Ambrosioides* Extract, supported by molecular docking analysis. *Arabian Journal of Chemistry*, 15, 103804.
- Amin, N.M., Noor, N.M. 2014. *Cosmos Caudatus* Kunth: A traditional medicinal herb. *Global Journal of Pharmacology*, 8, 420–426.
- Ansari, M.A, Murali, M., Prasad, D., Alzohairy, M.A., Almatroudi, A., Alomary, M.N., Udayashankar, A.C., Singh, S.B., Asiri, S.M.M., Ashwini, B.S., Gowtham, H.G., Kalegowda, N., Amruthesh, K.N., Lakshmeesha, T.R., Niranjana, S.R. 2020. Cinnamomum verum bark extract mediated green synthesis of ZnO nanoparticles and their antibacterial potentiality. *Biomolecules*, 10, 336.
- Aravind, M., Kumaresubitha, T., Ahmed, N., Velusamy, P. 2022. DFT, molecular docking, photocatalytic and antimicrobial activity of coumarin enriched cinnamon bark extract mediated silver nanoparticles. *Inorganic Chemistry Communications*, 146, 110176.
- Arumugam, J., Thambidurai, S., Suresh, S., Selvapandiyan, M., Kandasamy, M., Pugazhenthiran, N., Karthick Kumar, S., Muneeswaran, T., Quero, F. 2021. Green synthesis of zinc oxide nanoparticles using ficus carica leaf extract and their bactericidal and photocatalytic performance evaluation. *Chemical Physics Letters*, 783, 139040.
- Awasthi, K.K., Awasthi, A., Verma, R., Soni, I., Awasthi, K., John, P.J. 2015. Silver nanoparticles and carbon nanotubes induced DNA damage in mice evaluated by single cell gel electrophoresis. *Macromolecular Symposia*, 357, 210–217.
- Azwanida, Z.N., Jonathan, O.E., Melanie-Jaynes, H. 2020. Antioxidant, anti-collagenase, anti-elastase and anti-tyrosinase activities of an aqueous *cosmos caudatus* kunth (Asteraceae) leaf extract. *Tropical Journal of Natural Product Research*, 4, 1124–1130.
- Babayevska, N., Przysiecka, Ł., Iatsunskyi, I., Nowaczyk, G., Jarek, M., Janiszewska, E., Jurga, S. 2022. ZnO size and shape effect on antibacterial activity and cytotoxicity profile. *Scientific Reports*, 12, 8148.
- Barzinjy, A.A., Azeez, H.H. 2020. Green synthesis and characterization of zinc oxide nanoparticles using eucalyptus globulus labill. Leaf extract and zinc nitrate hexahydrate salt. *SN Applied Sciences*, 2, 991.
- Beasley, F.C., Vinés, E.D., Grigg, J.C., Zheng, Q., Liu, S., Lajoie, G.A., Heinrichs, D.E. 2009. Characterization of staphyloferrin A biosynthetic and transport mutants in *Staphylococcus aureus*. *Molecular Microbiology*, 72, 947–963.
- Boz, E., Stein, M. 2021. Accurate Receptor-Ligand Binding Free Energies from Fast QM Conformational Chemical Space Sampling. *International Journal of Molecular Sciences*, 22, 3078.
- Chakraborty, S., Farida, J.J., Simon, R., Kasthuri, S., Mary, N.L. 2020. Averrhoë carrambola fruit extract assisted green synthesis of ZnO nanoparticles for the photodegradation of congo red dye. *Surfaces and Interfaces*, 19, 100488.
- Daoud, A., Malika, D., Bakari, S., Hfaiedh, N., Mnafigui, K., Kadri, A., Gharsallah, N. 2019. Assessment of polyphenol composition, antioxidant and antimicrobial properties of various extracts of Date Palm Pollen (DPP) from two Tunisian cultivars. *Arabian Journal of Chemistry*, 12, 3075–3086.
- Debanath, M.K., Karmakar, S. 2013. Study of blueshift of optical band gap in zinc oxide (ZnO) nanoparticles prepared by low-temperature wet chemical method. *Materials Letters*, 111, 116–119.
- Elbrolesy, A., Abdou, F.A.E.Y., Morsy, R. 2024. Facile synthesis and biophysical characterization of novel Zinc Oxide / Fe₃O₄ Hybrid Nanocomposite as a potentially active agent in sunscreens. *Arabian Journal for Science and Engineering*, 49, 1083–1093.
- El-Fallal, A.A., Elfayoumy, R.A., El-Zahed, M.M. 2023. Antibacterial activity of biosynthesized zinc oxide nanoparticles using kombucha extract. *SN Applied Sciences*, 5, 332.
- Eswari, K.M., Asaithambi, S., Karuppaiah, M., Sakthivel, P., Balaji, V., Ponelakkia, D.K. 2022. Green synthesis of ZnO nanoparticles using *Abutilon Indicum* and *Tectona Grandis* leaf extracts for evaluation of anti-diabetic, anti-inflammatory and in-vitro cytotoxicity activities. *Ceramics International*, 48, 33624–33634.
- Firdaus, M.D., Artanti, N., Hanafi, M., Rosmalena. 2021. Phytochemical constituents and In vitro antidiabetic and

- antioxidant properties of various extracts of Kenikir (*Cosmos caudatus*) Leaves. *Pharmacognosy Journal*, 13, 890-895.
- Greeshma, K.P., Thamizselvi, R. 2022. Experimental and theoretical approach on green synthesized zinc oxide nanoparticles from combined leaf extracts of *Catharanthus Roseus* and *Morinda Citrifolia* for invitro anti-cancer studies. *Journal of Molecular Liquids*, 351, 118636.
- Hajiashrafi, S., Motakef-Kazemi, N. 2018. Green synthesis of zinc oxide nanoparticles using parsley extract. *Nanomedicine Research Journal*, 3, 44–50.
- Hudandini, M., Puri, N.R., Winardi, S., Widiyastuti, W., Shimada, M., Kusdianto, K. 2022. Photocatalytic activity of ZnO/Ag nanoparticles fabricated by a spray pyrolysis method with different O₂:N₂ carrier gas ratios and Ag contents. *Catalysts*, 12, 1374.
- Jayachandran, A., T.R., A., Nair, A.S. 2021. Green synthesis and characterization of zinc oxide nanoparticles using *Cayratia Pedata* Leaf Extract. *Biochemistry and Biophysics Reports*, 26, 100995.
- Jiang, J., Pi, J., Cai, J. 2018. The advancing of Zinc Oxide nanoparticles for biomedical applications. *Bioinorganic Chemistry and Applications*, 2018, 1–18.
- Kalam, A., Allami, S., Al-sehemi, A., Assiri, M., Yadav, P. 2022. Effect of stabilizer on optical band gap of ZnO and their performance in dye-sensitized solar cells. *Bulletin of the Chemical Society of Ethiopia*, 36, 209–222.
- Kamarajan, G., Anburaj, D.B., Porkalai, V., Muthuvel, A., Nedunchezian, G. 2022. Effect of temperature on optical, structural, morphological and antibacterial properties of biosynthesized ZnO nanoparticles. *Journal of the Nigerian Society of Physical Sciences*, 4, 892.
- Kanwal, S., Khan, M.T., Zaman, A., Tirth, V., Algahtani, A. 2023. Comparison the effect of co-precipitation and sol-gel techniques on the structural and magnetic attributes of ZnO and Zn(1-x)Fe0.05CoxO nanoparticles for attaining room temperature ferromagnetism (RTFM). *Digest Journal of Nanomaterials and Biostructures*, 18, 1025–37.
- Kusdianto, K., Sari, T.D., Laksono, M.A., Madhania, S., Winardi, S. 2021. Fabrication and application of ZnO-Ag nanocomposite materials prepared by gas-phase methods. *IOP Conference Series: Materials Science and Engineering*, 1053, 012023.
- Limón-Rocha, I., Guzmán-González, C.A., Anaya-Esparza, L.M., Romero-Toledo, R., Rico, J.L., González-Vargas, O.A., Pérez-Larios, A. 2022. Effect of the precursor on the synthesis of zno and its photocatalytic activity. *Inorganics*, 10, 1–17.
- Matinise, N., Fuku, X.G., Kaviyarasu, K., Mayedwa, N., Maaza, M. 2017. ZnO nanoparticles via *Moringa oleifera* green synthesis: Physical properties and mechanism of formation. *Applied Surface Science*, 406, 339–347.
- Mayedwa, N., Mongwaketsi, N., Khamlich, S., Kaviyarasu, K., Matinise, N., Maaza, M. 2018. Green synthesis of nickel oxide, palladium and palladium oxide synthesized via *Aspalathus linearis* natural extracts: physical properties and mechanism of formation. *Applied Surface Science*, 446, 266–272.
- Mayekar, J., Dhar, V., Radha, S. 2014. Role of salt precursor in the synthesis of zinc oxide nanoparticles. *International Journal of Research in Engineering and Technology*, 03, 43–45.
- McAuley, K.E., Svendsen, A., Patkar, S.A., Wilson, K.S. 2004. Structure of a feruloyl esterase from *Aspergillus niger*. *Acta Crystallographica Section D, Biological Crystallography*, 60, 878–887.
- Mendes, C.R., Dilarri, G., Forsan, C.F., Sapata, V. de M.R., Lopes, P.R.M., de Moraes, P.B., Montagnolli, R.N., Ferreira, H., Bidoia, E.D. 2022. Antibacterial action and target mechanisms of zinc oxide nanoparticles against bacterial pathogens. *Scientific Reports*, 12, 2658.
- Nagababu, U., Govindh, B., Diwakar, B. S., Kumar, G. K., Chatterjee, A. 2018. Synthesis andoptical charecterizationof luminescent ZnO NPs using *Tinospora Crispa* Stema- Green serspective. *Rasayan Journal of Chemistry*, 11, 1587–1593.
- Nandiyanto, A.B.D., Oktiani, R., Ragadhita, R. 2019. How to read and interpret FTIR spectroscopy of organic material. *Indonesian Journal of Science and Technology*, 4, 97–118.
- Nava, O.J., Soto-Robles, C.A., Gómez-Gutiérrez, C.M., Vilchis-Nestor, A.R., Castro-Beltrán, A., Olivás, A., Luque, P.A. 2017. Fruit peel extract mediated green synthesis of zinc oxide nanoparticles. *Journal of Molecular Structure*, 1147, 1–6.
- Nilavukkarasi, M., Vijayakumar, S., Prathipkumar, S. 2020. Materials science for energy technologies Capparis Zeylanica mediated bio-synthesized ZnO nanoparticles as antimicrobial, photocatalytic and anti-cancer applications. *Materials Science for Energy Technologies*, 3, 335–43.
- Nizamuddin, S., Hymavathi, A., Yaku, G., Umesh Kumar, U. 2022. Green synthesis and characterization of ZnO nanoparticles-a novel approach using *Carica Papaya* leaf extract. *Materials Today: Proceedings*, 62, 6854–6.
- Noriham, A., Dian-Nashiela, F., Kherni Hafifi, B., Nooraain, H., Azizah, A.H. 2015. Influences of maturity stages and extraction solvents on antioxidant activity of *Cosmos Caudatus* leaves, 3, 1–10.
- Osuntokun, J., Onwudiwe, D.C., Ebenso, E.E. 2019. Green synthesis of ZnO nanoparticles using aqueous *Brassica oleracea* L. var. *italica* and the photocatalytic activity. *Green Chemistry Letters and Reviews*, 12, 444–457.
- Owais Mushtaq, S., Sharma, R., Agrawal, A., Sharma, A., Kumar, S., Awasthi, K., Awasthi, A. 2022. Green synthesis of ZnO nanoparticles from Saffron Corm extract and their bactericidal activity. *Materials Today: Proceedings*, 69, 74–81.
- Pal, K., Chakroborty, S., Nath, N. 2022. Limitations of nanomaterials insights in green chemistry sustainable route : review on novel applications. *Green Processing and Synthesis*, 11, 951–964.
- Prasad, A.R., Basheer, S.M., Gupta, I.R., Elyas, K.K.,

- Joseph, A. 2020. Investigation on Bovine Serum Albumin (BSA) binding efficiency and antibacterial activity of ZnO nanoparticles. *Materials Chemistry and Physics*, 240, 122115.
- Qiu, X., Janson, C.A., Smith, W.W., Head, M., Lonsdale, J., Konstantinidis, A.K. 2001. Refined structures of β -ketoacyl-acyl carrier protein synthase IIII Edited by I. A. Wilson. *Journal of Molecular Biology*, 307, 341–356.
- Rajendrachari, S., Taslimi, P., Karaoglanli, A.C., Uzun, O., Alp, E., Jayaprakash, G.K. 2021. Photocatalytic degradation of Rhodamine B (RhB) dye in waste water and enzymatic inhibition study using cauliflower shaped ZnO nanoparticles synthesized by a novel One-pot green synthesis method. *Arabian Journal of Chemistry*, 14, 103180.
- Resmi, R., Yoonus, J., Beena, B. 2021. *Materials Today : Proceedings* A novel greener synthesis of ZnO nanoparticles from Nilgiri antuscilantus leaf extract and evaluation of its biomedical applications. *Materials Today: Proceedings*, 46, 3062–3068.
- Roxy M.S., Ananthu A., Sumithranand V. 2021. Synthesis and characterization of undoped and magnesium doped zinc oxide nanoparticles. *International Journal of Scientific Research in Science and Technology*, 8, 134–139.
- Saad, B.L., Soltane, L., Sediri, F. 2019. Pure and Cu-doped ZnO nanoparticles: hydrothermal synthesis, structural, and optical properties. *Russian Journal of Physical Chemistry A*, 93, 2782–8.
- Sadiq, H., Sher, F., Sehar, S., Lima, E.C., Zhang, S., Iqbal, H.M.N., Nuhanović, M. 2021. Green synthesis of ZnO nanoparticles from Syzygium Cumini leaves extract with robust photocatalysis applications. *Journal of Molecular Liquids*, 335, 116567.
- Saha, R., Subramani, K., Sikdar, S., Fatma, K., Rangaraj, S. 2021. Effects of processing parameters on green synthesised zno nanoparticles using stem extract of swertia chirayita. *Biocatalysis and Agricultural Biotechnology*, 33, 101968.
- Sangeetha, G., Rajeshwari, S., Rajendran, V. 2011. Green synthesis of zinc oxide nanoparticles by aloe barbadensis miller leaf extract: structure and optical properties. *Materials Research Bulletin*, 46, 2560–2566.
- Sasi, S., Fathima Fasna, P.H., Bindu Sharmila, T.K., Julie Chandra, C.S., Antony, J.V., Raman, V., Ramanathan, H.N. 2022. Green synthesis of ZnO nanoparticles with enhanced photocatalytic and antibacterial activity. *Journal of Alloys and Compounds*, 924, 166431.
- Sharma, D., Thakur, N., Vashist, J., Bisht, G.S. 2018. Antibacterial evaluation of cuprous oxide nanoparticles synthesized using leaf extract of Callistemon Viminalis. *Indian Journal of Pharmaceutical Education and Research*, 52, 449–455.
- Tangkawanit, S., Culshaw, E.V., Keawsri, P. 2023. Enhancing cotton fabrics properties by coating with zinc oxide and carbon black nanomaterial and dyeing with terminalia Catappa Leaves Powder. *Applied Science and Engineering Progress*, 16, 5868.
- Thiruganasambantham, T., Thiagamani, S.M.K., Natarajan, H., Siengchin, S., Rangappa, S.M. 2023. Fabrication and characterization of an active nanocomposite film based on polystyrene/thyme ZnO for food packaging. *Applied Science and Engineering Progress*, 16, 6440.
- Vasquez, R.D., Apostol, J.G., de Leon, J.D., Mariano, J.D., Mirhan, C.M.C., Pangan, S.S., Reyes, A.G.M., Zamora, E.T. 2016. Polysaccharide-mediated green synthesis of silver nanoparticles from Sargassum Siliquosum J.G. Agardh: assessment of toxicity and hepatoprotective activity. *OpenNano*, 1, 16–24.
- Velsankar, K., Sudhakar, S., Maheshwaran, G., Krishna Kumar, M. 2019. Effect of biosynthesis of ZnO nanoparticles via Cucurbita Seed extract on Culex Tritaeniorhynchus Mosquito Larvae with its biological applications. *Journal of Photochemistry and Photobiology B: Biology*, 200, 111650.
- Vijayakumar, S., Arulmozhi, P., Kumar, N., Sakthivel, B., Prathip Kumar, S., Praseetha, P.K. 2020. Acalypha fruticosa L. leaf extract mediated synthesis of ZnO nanoparticles: characterization and antimicrobial activities. *Materials Today: Proceedings*, 23, 73–80.
- Vinayagam, R., Sharma, G., Murugesan, G., Pai, S., Gupta, D., Narasimhan, M.K., Selvaraj, R. 2022. Rapid photocatalytic degradation of 2, 4-dichlorophenoxy acetic acid by ZnO nanoparticles synthesized using the leaf extract of Muntingia calabura. *Journal of Molecular Structure*, 1263, 133127.
- Visveshwari M., Subbaiyan B., Thangapandian V. 2018. Phytochemical analysis, antibacterial activity, FTIR and GCMS analysis of Ceropogia juncea Roxb. *International Journal of Pharmacognosy and Phytochemical Research*, 9, 914–920.
- Yang, H., Zhang, J., Li, Z., Huang, J., Wu, J., Zhang, Y., Ge, H. 2023. antibacterial effect of low-concentration ZnO nanoparticles on sulfate-reducing bacteria under visible light. *Nanomaterials*, 13, 2033.
- Zeghoud, S., Hemmami, H., Ben, B., Ben, I., Kouadri, I., Rebiai, A., Messaoudi, M., Ahmed, S. 2022. A review on biogenic green synthesis of ZnO nanoparticles by plant biomass and their applications. *Materials Today Communications*, 33, 104747.
- Zhu, W., Hu, C., Ren, Y., Lu, Y., Song, Y., Ji, Y., He, J. 2021. Green synthesis of zinc oxide nanoparticles using Cinnamomum camphora (L.) Presl leaf extracts and its antifungal activity. *Journal of Environmental Chemical Engineering*, 9, 106659.